Journal of Materials Chemistry A

PAPER

View Article Online
View Journal | View Issue

CrossMark click for updates

Cite this: J. Mater. Chem. A, 2016, 4, 6639

"Water-in-Salt" electrolytes enable green and safe Li-ion batteries for large scale electric energy storage applications†

Liumin Suo,[a] Fudong Han,[a] Xiulin Fan,[a] Huili Liu,[a] Kang Xu*[b] and Chunsheng Wang*[a]

Received 16th January 2016
Accepted 17th February 2016

DOI: 10.1039/c6ta00451b

www.rsc.org/MaterialsA

Although state-of-the-art Li-ion batteries have overwhelmed the market of portable electronics as the main power source, their intrinsic limitations imposed by concerns over their safety, toxicity and cost have prevented them from being readily adopted by large-scale electric energy storage applications. Leveraging the new class of aqueous electrolytes of wide electrochemical stability window to resolve these concerns, we describe a new aqueous Li-ion chemistry based on $LiFePO_4$/water-in-salt/Mo_6S_8 that is safe, green and economical. These merits, along with superior electrochemical performances such as excellent cycling stability (>1000 cycles), both high coulombic and round-trip efficiencies, high rate capability, low self-discharge rate at the fully charged state, as well as a wide service temperature range (−20 to +55 °C), make this new battery chemistry a promising candidate in energy storage units for large-scale applications.

Introduction

As energy storage units, rechargeable batteries are indispensable components in almost any power system, from electric vehicles to smart grids that harvest energy from intermittent sources such as solar, wave or wind.[1–3] Possessing a very high energy density, Li-ion batteries have been considered as primary candidates for such applications; however, their intrinsic limitations arising from safety, environmental impact and cost have prevented them from being readily adopted in those large-scale applications (1000–1 000 000 W h). A closer examination reveals that most of these concerns originated from the non-aqueous electrolytes used in the state-of-the-art Li-ion batteries. Based on lithium salts containing labile phosphorus–fluorine bonds dissolved in organic carbonate esters, these electrolytes are inflammable, toxic especially when the batteries experience thermal runaway,[4] and incur high cost not only directly from the manufacturing, processing and transportation processes of these moisture-sensitive materials, but to an even greater degree from the packaging and safety management of large battery modules and packs.[5–7]

Replacing the non-aqueous electrolytes with an aqueous alternative would resolve all these concerns;[8–12] however, the narrow electrochemical stability window of aqueous electrolytes (<1.5 V), often defined by the evolution of hydrogen at negative electrode and oxygen at positive electrode surfaces, prevented the use of most Li-ion electrochemical couples, which usually generate a cell voltage of >3.0 V. Such an intrinsic limitation, imposed by the potentials where water decomposes into hydrogen and oxygen, constitutes a major obstacle to any attempts of fabricating an aqueous Li-ion battery of high voltage (>2.0 V) and energy density (>50 W h kg^{-1}).[13–19] Even when operating under 1.5 V, most of these systems are still plagued by high self-discharge rates and poor storage stabilities, as revealed by the fact that in the literature the aqueous batteries were often cycled at high rates to camouflage the effect of parasitic reactions on cycling stability.

Recently, a new class of aqueous electrolytes was reported by Suo *et al.*, who managed to form a solid-electrolyte-interphase (SEI) for the first time in aqueous media by manipulating the structure of a Li^+-solvation sheath.[20] The presence of such an aqueous SEI successfully expanded the electrochemical stability window of aqueous electrolytes from ~1.23 V to nearly 3.0 V, thus enabling many Li-ion chemistries that are otherwise impossible. A 2.3 V full Li-ion cell using the electrochemical couple of $LiMn_2O_4$/Mo_6S_8 was demonstrated in such an electrolyte, delivering over 1000 cycles at a projected energy density of ~100 W h kg^{-1}.[20] However, the positive electrode selected therein ($LiMn_2O_4$) is known for its persisting fading behavior in non-aqueous electrolytes, which occurred at least partially *via* the so-called Jahn–Teller effect arising from the thermodynamic instability of the spinel lattice. This degradation process would accelerate at elevated temperatures (55 °C).[21,22] To seek a more electrochemically stable positive electrode that targets the grid-

[a]Department of Chemical and Biomolecular Engineering, University of Maryland College Park, Maryland, 20740, USA. E-mail: cswang@umd.edu

[b]Electrochemistry Branch, Sensor and Electron Devices Directorate, Power and Energy Division U.S. Army Research Laboratory Adelphi, Maryland, 20783, USA. E-mail: conrad.k.xu.civ@mail.mil

† Electronic supplementary information (ESI) available. See DOI: 10.1039/c6ta00451b

storage applications, where safety, environmental and cost concerns far outweigh the gravimetric or volumetric energy densities, we turned our attention to $LiFePO_4$. The olivine lattice structure of this positive material has been known for its thermal stability, non-toxicity, safety and low cost.[23,24] Previously, $LiFePO_4$ has been used in aqueous electrolytes due to its moderate lithiation/de-lithiation potential (3.5 V *vs.* Li).[25–27] However, on one hand, in alkaline electrolytes and in the presence of dissolved oxygen, $LiFePO_4$ became unstable during charging;[28] on the other hand, restricted by the narrow electrochemical stability window of aqueous electrolytes and the consequent limited choice of anode materials, the output voltage of aqueous Li-ion full cells using $LiFePO_4$ is constantly less than 1.0 V, making the benefits of such aqueous alternatives marginal.[15] With the ability to form a SEI in aqueous media, the new "Water-in-Salt" electrolyte significantly relaxed the cathodic restrictions from 2.6 V to 1.9 V (*vs.* Li), hence allowing the use of anode materials with redox potentials below 2.6 V, such as chevrel phase Mo_6S_8. Furthermore, under neutral conditions (pH $\sim$ 7.0), the resistance against oxygen dissolution, non-corrosive nature and wide working temperature range of the new electrolyte not only ensured the reversibility of $LiFePO_4$ but also introduced additional packaging and environmental benefits to the manufacturing and processing of the cells and materials. The combination of electrochemical coupling of $LiFePO_4$, Mo_6S_8 and "Water-in-Salt" electrolyte would lead to a full Li-ion cell chemistry of 1.3 V with expected merits arising from all three materials: non-toxicity, high safety, excellent cycling and thermal stability, high coulombic and round-trip efficiencies, wide service temperature range, high rate capability and storage stability. These advantages would undoubtedly result in a system that best suits the key requirements of large scale energy storage units.

Experimental

Materials

The chevrel phase Mo_6S_8 was prepared by leaching Cu from copper chevrel powder $CuMo_3S_4$ that was synthesized *via* solid-state synthesis. CuS (99% Sigma-Aldrich), Mo (99.99% Sigma-Aldrich), MoS_2 (99% Sigma-Aldrich) were ground by ball-milling for 0.5 h, and then the powder was pelleted at 10 MPa and sealed in a stainless steel Swagelok cell, which was heated to 900 °C for 24 h at a heating rate of 2 °C min^{-1} in argon. The products were placed and stirred in a 6 M HCl solution for 12 h with O_2 bubbling to remove Cu. Finally, the obtained chevrel powder (Mo_6S_8) was washed with deionized water three times under vacuum filtration followed by drying at 100 °C overnight. $LiFePO_4$ was purchased from A123 Corporation.

Materials characterization

X-ray diffraction patterns were recorded on a D8 Advance X-ray diffractometer (Bruker), with Cu Kr radiation in the 2-theta range of 10–90 degree. Scanning electron microscopy (SEM) was conducted on a Hitachi S-4700 (Japan) operating at 10 kV, and transmission electron microscopy (TEM) on a Hitachi S-4700 (Japan) operating at 10 kV and in a JEOL (Japan) 2100F field emission TEM, respectively. X-ray photoelectron spectroscopy (XPS) analysis was performed on a high resolution Kratos AXIS 165 X-ray photoelectron spectrometer using monochromic AlKa radiation.

Electrochemical measurements

The electrodes were fabricated by compressing active materials, carbon black, poly(vinylidene difluoride) (PTFE) at the weight ratio of 8 : 1 : 1 on a stainless steel grid before electrochemical performance measurements. The aqueous "Water-in-Salt" electrolyte (the weight and volume ratio of LiTFSI to water is above 1) was made by making a 21 m solution of lithium bis(trifluoromethane sulfonyl)imide (LiTFSI) in de-ionized H_2O. Cyclic voltammetry (CV) was carried out using a CHI 600E electrochemical work station and three-electrode cells. The CV of $LiFePO_4$ was conducted with $LiFePO_4$ as working, excessive active black (AB) as counter and Ag/AgCl as reference electrodes, respectively. The CV of Mo_6S_8 was conducted with Mo_6S_8 as the working electrode, a 2 mm platinum disk as the counter electrode and Ag/AgCl as reference electrodes. The potentials referring to the Ag/AgCl reference electrode were converted to Li^+/Li for convenience. CV was also applied to determine the electrochemical stability window of electrolytes using electrochemically inert electrodes (316 stainless steel grid, 200-mesh sieve) as working and counter electrodes. They were thoroughly cleaned with high purity alcohol under ultrasonic agitation, followed by washing with high purity water three times and then drying before measurements. The full Li-ion cells were assembled in a CR2032-type coin cell configuration with the $LiFePO_4$ as the positive electrode, Mo_6S_8 as the negative electrode and a glass fiber as the separator. The active mass ratio of $LiFePO_4$ to Mo_6S_8 was set to be 2 : 1. The galvanostatic cycling was carried out on a Land BT2000 battery test system (Wuhan, China) at room-temperature (25 °C).

Results and discussion

The excellent cycling stability of $LiFePO_4$ in both non-aqueous and aqueous electrolytes has been reported in previous literature.[15,29] In this work we selected a commercial $LiFePO_4$ material from A123, whose XRD and SEM images are shown in Fig. S1 and S2,† respectively. The crystal structure and morphology of Mo_6S_8 at either pristine (Mo_6S_8) or fully-lithiated ($Li_4Mo_6S_8$) states are shown in Fig. 1. Apparently the Mo_6S_8 unit in chevrel phase can be considered as an octahedron of Mo atoms in a cube of S atoms, and the chevrel phase arranges with the Mo_6S_8 clusters tilted relatively to each other, in which a large number of sites exist among clusters that constitute diffusion channels for ion transport. Thus, chevrel phase Mo_6S_8 has high electronic and ionic conductivities, making it a suitable electrode for both Li^+ and Mg^{2+} intercalations.[30,31] The XRD pattern in Fig. 1d reveals the Mo_6S_8 sample as a pure chevrel phase (space group: $R\bar{3}$ and JCPDS-ICDD: 00-027-0319) after the as-prepared $Cu_2Mo_6S_8$ was etched with HCl. To confirm the chevrel phase, the surface chemistry of Mo_6S_8 was investigated by XPS (Fig. 1f). The characteristic twin peaks for both Mo and S shell

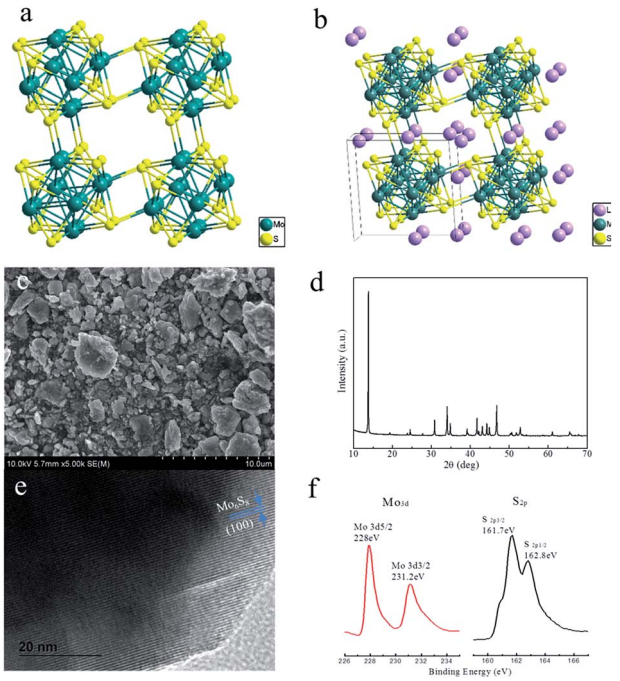

Fig. 1 The chevrel phase Mo_6S_8. (a) and (b) The crystal structures of Mo_6S_8 and $Li_4Mo_6S_8$, (c) and (d) SEM and high resolution TEM images of pristine Mo_6S_8, (e) X-ray pattern of Mo_6S_8 and (f) XPS spectra of Mo_6S_8.

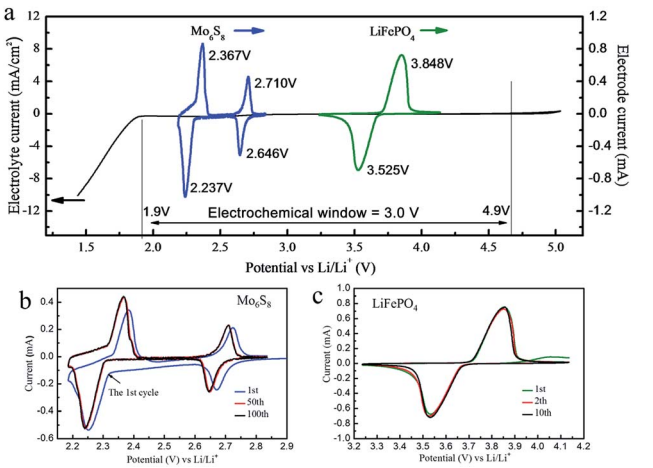

Fig. 2 Cycling voltammetry (CV) of the electrodes and electrolyte materials. (a) The electrochemical stability window of the water-in-salt electrolyte as measured on the inert current collector (stainless steel grid) at a scanning rate of 10 mV s^{-1}, which is overlaid with the 1st CV traces of active anode (Mo_6S_8) and positive ($LiFePO_4$) materials measured at a scanning rate of 0.1 mV s^{-1} in the same electrolyte, (b) the evolution of CV traces of the chevrel phase Mo_6S_8 and (c) olivine $LiFePO_4$ at a scanning rate of 0.1 mV s^{-1}.

electrons (Mo_{3d} and S_{2p}) are identified at the expected binding energies ($Mo_{3d5/2} \sim 228$ eV, $Mo_{3d3/2} \sim 231.2$ eV and $S_{2p3/2} \sim 161.7$ eV, $S_{2p1/2} \sim 162.8$ eV).

A three-electrode cell was used to evaluate the compatibility and reversibility of $LiFePO_4$ or Mo_6S_8 in the concentrated aqueous electrolyte. As Fig. 2a shows, the expanded electrochemical window of the novel aqueous electrolyte is sufficiently wide to support the electrochemical coupling of $LiFePO_4$ and Mo_6S_8. As described in our earlier report, the increased Li^+-activity due to the high LITFSI concentration shifts the redox potentials positively, but the potential difference between the positive electrode and negative electrode (*i.e.*, the cell voltage) remains constant at all salt concentrations. The evolution of CV for Mo_6S_8 and $LiFePO_4$ is shown in Fig. 2b and c, verifying the high reversibility of these electrode materials. In particular (Fig. 2b), Mo_6S_8 shows nearly zero fading within 100 cycles by CV at a slow scanning rate (0.1 mV s^{-1}), with the exception of the 1st cycle where part of the irreversible lithium consumption was caused by SEI formation. Since the redox potential of this negative electrode lies beyond the hydrogen evolution potential of the salt-in-water aqueous electrolyte under neutral conditions (2.63 V *vs.* Li), this stability highlights the excellent protective effect of the formed SEI.

The performance of this electrochemical couple was further evaluated in the same three-electrode cells, in which the negative electrode and positive electrode were subject to constant current cycling at different rates in the presence of an independent Ag/AgCl reference electrode (Fig. 3). In this manner both the voltage of the full cell as well as potentials of individual electrodes (relative to Li^+/Li) can be monitored simultaneously. To evaluate how stable the electrolyte is in contact with these electrodes, both low and high rates (0.20C and 1C) were used. As Fig. 3a shows, $LiFePO_4$ presents one plateau (charge: 3.69 V and discharge: 3.64 V) and Mo_6S_8 displays two plateaus (charge: 2.38 V and 2.74 V and discharge: 2.71 V and 2.33 V), which consequently lead to two distinct discharge plateaus for the full cell at 1.3 V and 0.9 V (Fig. 3b). To compensate for the irreversible loss caused by SEI formation, we set the ratio of $LFePO_4$ to Mo_6S_8 to be 2 : 1 by weight. The electrochemical performance of the $LiFePO_4$/Mo_6S_8 full cell was tested in coin cells and is shown in Fig. 4. As shown in Fig. 4a, the formation process of the SEI should complete within 10 cycles, after which a coulombic efficiency above 96% was achieved at 0.20C. Considering that the negative electrode actually operates at a potential below that of hydrogen evolution, this high coulombic efficiency achieved at this low rate is unprecedented.

Based on the first discharge data normalized by the total mass of both positive and negative electrodes, the full Li-ion cell delivers an energy density of 47 W h kg^{-1}. The charge/discharge

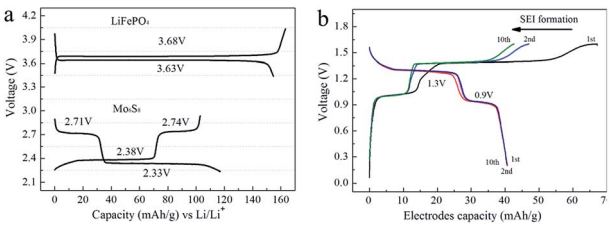

Fig. 3 The charge–discharge profiles. (a) The typical voltage profiles of $LiFePO_4$ and Mo_6S_8 electrodes in three-electrode devices at a constant current (0.2C) and (b) the voltage profiles of full-cell configuration ($LiFePO_4$/Mo_6S_8) at a constant current (0.2C).

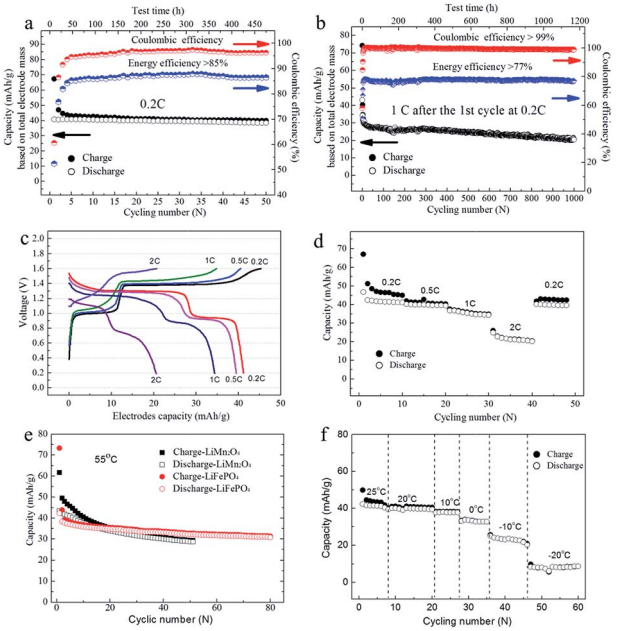

Fig. 4 Electrochemical performances of the full Li-ion cell based on $LiFePO_4/Mo_6S_8$. (a) and (b) The cycling stability, round trip energy efficiencies and coulombic efficiencies of the full Li-ion cell at low (0.2C) and high (1C) rates respectively; (c) and (d) the rate capability at room temperature; (e) the comparison of elevated temperature cycling stability (55 °C) between $LiFePO_4$ and $LiMn_2O_4$; (f) low temperature cycling stability from 25 °C to −20 °C. All the capacity shown in the figure is calculated based on the total electrode masses of $LiFePO_4$ and Mo_6S_8.

efficiencies at 0.2C and 1C, calculated by the energy the full cell absorbs and releases, are also plotted in Fig. 4a and b. It shows high round-trip efficiencies with >85% at 0.2C and >77% at 1C respectively. At a low rate (0.2C), after 50 cycles and 20 days of testing time, the full Li-ion cells still retain 94.3% of the initial capacity (the first discharge: 40.7 mA h g^{-1} and the 50th discharge: 38.4 mA h g^{-1}). At a high rate (1C), cycling life readily lasts over 1000 cycles (the testing time: about 49 days) with a low fading rate of 0.04% per cycle and high coulombic efficiency above 99%. Although the LiTFSI concentration is up to 21 m, the Li-ion conductivity of the water-in-salt electrolyte is still higher than 10^{-2} S cm^{-1},[12] allowing high rate performance as shown in Fig. 4c and d. The electrochemical performances were also evaluated at different temperatures that the nature could impose to a large-scale grid-storage system, from +55 °C down to −20 °C (Fig. 4e and f). Apparently, at 55 °C the $LiFePO_4/Mo_6S_8$ full cell outperformed $LiMn_2O_4/Mo_6S_8$ in cycling stability, while the latter demonstrated a rapid capacity fading, the reason underneath might be the well-known Jahn–Teller transformation and subsequent Mn dissolution accelerated by the high temperature (55 °C). On the other hand, with the temperature decreasing from 25 °C to −20 °C stepwise (Fig. 4d), the delivered capacity of full Li-ion cell decreased accordingly; however, even at −20 °C, the cell still cycles as evidenced by the voltage profiles shown in Fig. S3.†

It has been widely believed that long cycling life is difficult to achieve for aqueous Li-ion batteries, especially at rates lower than 1C, even when the operating potential of negative materials lies within the thermodynamic stability of water (<1.5 V). The rationale for this instability originates from the fact that the hydrogen evolution occurs at fast kinetics that cannot be readily delayed. In the literature describing the cycling behavior of aqueous Li-ion cells, high rates (>1C) were almost exclusively used in order to minimize the effect of hydrogen evolution on capacity retention. Such tactical approaches, however, could be misleading, because as Dahn and coworkers demonstrated that the real stability does not come from the number of cycles but from the duration that a system stays at the fully charged state, or from the coulombic efficiencies observed at low cycling rates.

In this context, the superior cycling stability demonstrated at 0.20C in our work using a negative electrode that operates beyond the hydrogen evolution potential underlines the effectiveness of the formed SEI. One primary mission for large-scale grid-storage batteries is how well the harvested energy could be kept at the fully charged state (100% state-of-charge, or SOC) during the storage phase. In order to evaluate the storage performance of the aqueous $LiFePO_4/Mo_6S_8$ full cell, we employed two different approaches. We first monitored the decay of open circuit voltage (OCV) at 100% OCV (Fig. 5a), because the negative electrode at the fully lithiated state is most electrochemically active, and most of the parasitic reactions occurring thereon could be the source of self-discharge. Fig. 5a shows a negligible potential change, which remains above 1.32 V after 20 days, and then it drops to 0.96 V. In the worst case, if we assume that all capacity loss during this storage period is entirely incurred by the parasitic

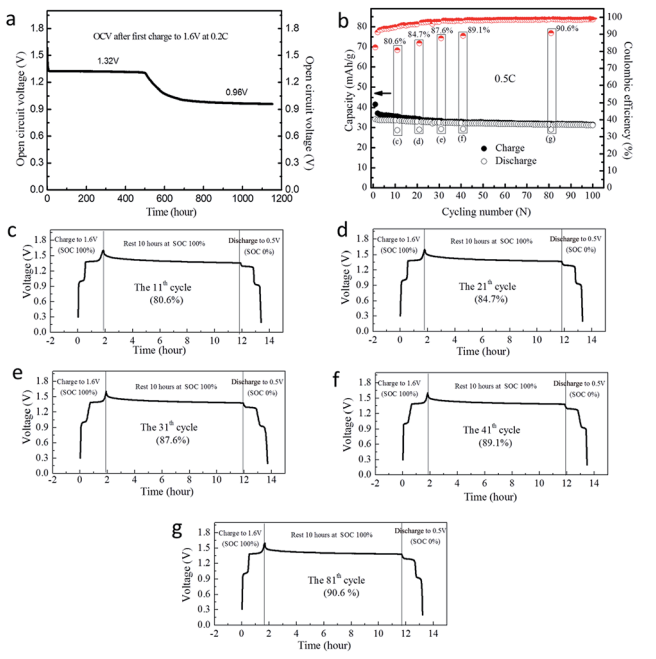

Fig. 5 Electrochemical storage of the full cell based on $LiFePO_4/Mo_6S_8$. (a) The OCV decay at the fully charged state of 1.6 V at 0.2C, (b) the cycling performances at 0.5C with a 10 hour rest after every 10 or 50 cycles. The self-discharge was evaluated by comparison with the columbic efficiency and the capacity loss after resting. (c)–(g) The voltage profiles of charging and discharging immediately before and after the 10 hour rest.

reactions at the Mo_6S_8 anode side alone, and that the theoretical capacity of the Mo_6S_8 anode in the first discharge plateau is about 85 mA h g^{-1} (128 mA h g^{-1} × 2/3 = 85 mA h g^{-1}) (Fig. 3a), then the self-discharge rate of the full Li-ion cell is estimated to be less than 0.13% per hour at 100% SOC, which is the lowest among those of all reported aqueous rechargeable Li-ion systems so far. Since these data are obtained from non-optimized coin cells fabricated in laboratory, experience tells us that there is much space for further improvement *via* cell design and engineering. The low self-discharge rate of the $LiFePO_4/Mo_6S_8$ full cell at beyond the hydrogen evolution potential is attributed to the protection by the formed SEI. Secondly, we attempted to correlate SEI formation with the self-discharge rate. We cycled the cell continuously and then placed it on a 10 hour rest at 100% SOC every 10 cycles, before cycling resumes. The capacity loss between charge and discharge cycles after the 10 hour rest could reveal any self-discharge behavior of the full Li-ion cell (Fig. 5b). As shown in Fig. 5b, the coulombic efficiencies among the cycles interrupted by the rest steadily increase with the cycle number, *e.g.*, 80.6% at the 11^{th} cycle: 84.7% at the 21^{th} cycle, 87.6% at the 31^{th} cycle, and 89.1% at the 41^{th} cycle. We believe that the trend of coulombic efficiency actually reflects the gradual formation process of a SEI at the anode, which becomes more and more effective in protecting the anode surface against parasitic hydrogen evolution reactions. The voltage profiles of the charging and discharging processes immediately before or after each 10 hour rest (Fig. 5c–g) clearly reveal this evolution process which stabilizes after 80 cycles with above 90% coulombic efficiency after resting for 10 hours at 100% SOC. By this time, we believe that SEI formation is almost completed. Overall, SEI formation is determined by both charge–discharge time and cycles. Thus, as Fig. 4b shows, the batteries could be first formed at a low rate (0.2C) during the initial cycles, and then subjected to high rates. In this case, nearly 100% coulombic efficiency could be achieved after 10 cycles, which indicates the suitability of the system for energy storage applications.

Conclusions

In summary, we report a safe, green and low cost aqueous Li-ion battery chemistry that targets the large-scale energy storage applications. The full Li-ion cell based on the $LiFePO_4$/"Water-in-Salt" electrolyte/Mo_6S_8 combines advantages of state-of-the-art Li-ion batteries (long cycling life, high round-trip efficiency and low maintenance) and aqueous batteries (low production cost, green and high safety). Its superior cycling reversibility (>1000 cycles) at both low (0.2C) and high (1C) rates with high coulombic efficiency, along with durability against extreme temperatures from −20 to 55 °C and excellent storage retention at the fully charged state, make it a competitive candidate for energy-harvesting smart-grids.

Acknowledgements

The work was supported by DOE ARPA-E (DEAR0000389). We also acknowledge the support of the Maryland Nano Center and its NispLab. The NispLab is supported in part by the NSF as a MRSEC Shared Experimental Facility.

Notes and references

1 B. Dunn, H. Kamath and J.-M. Tarascon, *Science*, 2011, **334**, 928–935.
2 Z. Yang, J. Zhang, M. C. W. Kintner-Meyer, X. Lu, D. Choi, J. P. Lemmon and J. Liu, *Chem. Rev.*, 2011, **111**, 3577–3613.
3 H. Pan, Y.-S. Hu and L. Chen, *Energy Environ. Sci.*, 2013, **6**, 2338–2360.
4 A. Hammami, N. Raymond and M. Armand, *Nature*, 2003, **424**, 635–636.
5 J. M. Tarascon and M. Armand, *Nature*, 2001, **414**, 359–367.
6 K. Xu, *Chem. Rev.*, 2004, **104**, 4303–4417.
7 K. Xu, *Chem. Rev.*, 2014, **114**, 11503–11618.
8 W. Yang, K. Kang, H. Li, X.-Q. Yang, L. Chen and X. Huang, *Nat. Commun.*, 2015, **6**, 6401.
9 M. Pasta, C. D. Wessells, R. A. Huggins and Y. Cui, *Nat. Commun.*, 2012, **3**, 1149.
10 Y. Wang, J. Yi and Y. Xia, *Adv. Energy Mater.*, 2012, **2**, 830–840.
11 C. Wessells, R. A. Huggins and Y. Cui, *J. Power Sources*, 2011, **196**, 2884–2888.
12 H. Kim, J. Hong, K.-Y. Park, H. Kim, S.-W. Kim and K. Kang, *Chem. Rev.*, 2014, **114**, 11788–11827.
13 W. Li, J. R. Dahn and D. S. Wainwright, *Science*, 1994, **264**, 1115–1118.
14 W. Tang, Y. Zhu, Y. Hou, L. Liu, Y. Wu, K. P. Loh, H. Zhang and K. Zhu, *Energy Environ. Sci.*, 2013, **6**, 2093–2104.
15 J.-Y. Luo, W.-J. Cui, P. He and Y.-Y. Xia, *Nat. Chem.*, 2010, **2**, 760–765.
16 C. Wessells, R. Ruffo, R. A. Huggins and Y. Cui, *Electrochem. Solid-State Lett.*, 2010, **13**, A59–A61.
17 R. Ruffo, C. Wessells, R. A. Huggins and Y. Cui, *Electrochem. Commun.*, 2009, **11**, 247–249.
18 Q. T. Qu, L. J. Fu, X. Y. Zhan, D. Samuelis, J. Maier, L. Li, S. Tian, Z. H. Li and Y. P. Wu, *Energy Environ. Sci.*, 2011, **4**, 3985–3990.
19 W. Tang, L. L. Liu, Y. S. Zhu, H. Sun, Y. P. Wu and K. Zhu, *Energy Environ. Sci.*, 2012, **5**, 6909–6913.
20 L. Suo, O. Borodin, T. Gao, M. Olguin, J. Ho, X. Fan, C. Luo, C. Wang and K. Xu, *Science*, 2015, **350**, 938–943.
21 D. H. Jang, Y. J. Shin and S. M. Oh, *J. Electrochem. Soc.*, 1996, **143**, 2204–2211.
22 Y. Y. Xia, Y. H. Zhou and M. Yoshio, *J. Electrochem. Soc.*, 1997, **144**, 2593–2600.
23 D. Choi, D. Wang, V. V. Viswanathan, I.-T. Bae, W. Wang, Z. Nie, J.-G. Zhang, G. L. Graff, J. Liu, Z. Yang and T. Duong, *Electrochem. Commun.*, 2010, **12**, 378–381.
24 X.-L. Wu, L.-Y. Jiang, F.-F. Cao, Y.-G. Guo and L.-J. Wan, *Adv. Mater.*, 2009, **21**, 2710–2714.
25 C. H. Mi, X. G. Zhang and H. L. Li, *J. Electroanal. Chem.*, 2007, **602**, 245–254.
26 Y. Hou, X. Wang, Y. Zhu, C. Hu, Z. Chang, Y. Wu and R. Holze, *J. Mater. Chem. A*, 2013, **1**, 14713–14718.

27 P. He, X. Zhang, Y.-G. Wang, L. Cheng and Y.-Y. Xia, *J. Electrochem. Soc.*, 2008, **155**, A144–A150.
28 M. Minakshi, S. Pritam, T. Stephen and P. Kathryn, *J. Power Sources*, 2006, **158**, 646–649.
29 M. Takahashi, H. Ohtsuka, K. Akuto and Y. Sakurai, *J. Electrochem. Soc.*, 2005, **152**, A899–A904.
30 P. J. Mulhern and R. R. Haering, *Can. J. Phys.*, 1984, **62**, 527–531.
31 D. Aurbach, Z. Lu, A. Schechter, Y. Gofer, H. Gizbar, R. Turgeman, Y. Cohen, M. Moshkovich and E. Levi, *Nature*, 2000, **407**, 724–727.